



Structural and Biochemical Study of the Mono-ADP-Ribosyltransferase Domain of SdeA, a Ubiquitylating/Deubiquitylating Enzyme from *Legionella pneumophila*

Leehyeon Kim¹, Do Hoon Kwon¹, Bong Heon Kim¹, Jiyeon Kim², Mi Rae Park¹, Zee-Yong Park² and Hyun Kyu Song¹

¹ - Department of Life Sciences, Korea University, 145 Anam-ro, Seongbuk-gu, Seoul 02841, Korea

² - School of Life Sciences, Gwangju Institute of Science and Technology, Gwangju 61005, Korea

Correspondence to Hyun Kyu Song: hksong@korea.ac.kr

<https://doi.org/10.1016/j.jmb.2018.05.043>

Edited by John Johnson

Abstract

Conventional ubiquitylation occurs through an ATP-dependent three-enzyme cascade (E1, E2, and E3) that mediates the covalent conjugation of the C-terminus of ubiquitin to a lysine on the substrate. SdeA, which belongs to the SidE effector family of *Legionella pneumophila*, can transfer ubiquitin to endoplasmic reticulum-associated Rab-family GTPases in a manner independent of E1 and E2 enzymes. The novel ubiquitin-modifying enzyme SdeA utilizes NAD⁺ as a cofactor to attach ubiquitin to a serine residue of the substrate. Here, to elucidate the coupled enzymatic reaction of NAD⁺ hydrolysis and ADP-ribosylation of ubiquitin in SdeA, we characterized the mono-ADP-ribosyltransferase domain of SdeA and show that it consists of two sub-domains termed mART-N and mART-C. The crystal structure of the mART-C domain of SdeA was also determined in free form and in complex with NAD⁺ at high resolution. Furthermore, the spatial orientations of the N-terminal deubiquitylase, phosphodiesterase, mono-ADP-ribosyltransferase, and C-terminal coiled-coil domains within the 180-kDa full-length SdeA were determined. These results provide insight into the unusual ubiquitylation mechanism of SdeA and expand our knowledge on the structure–function of mono-ADP-ribosyltransferases.

© 2018 Elsevier Ltd. All rights reserved.

Introduction

Post-translational modification of proteins by ubiquitin (Ub) is one of the most common protein modifications and is involved in numerous key cellular processes in eukaryotes [1–3]. Ubiquitylation is mediated by a three-enzyme cascade (E1 Ub activation, E2 Ub conjugation, and E3 Ub ligation) and results in the covalent conjugation of Ub to a lysine residue on the substrate [4–6]. Differently linked Ub chains have unique structural features and mediate distinct cellular functions including proteasomal degradation, autophagy, innate and adaptive immunity, and defense against pathogens [4, 6–10]. Given the essential regulatory roles of Ub signaling pathways in eukaryotes, invaders such as bacterial pathogens and viruses developed mechanisms to hijack host Ub signaling pathways to evade the immune response [11–14]. The ubiquitylation network is therefore a common target for diverse infectious pathogens [15]. Bacteria secrete two different types of protein to modulate the host Ub network, namely, ubiquitylating

and deubiquitylating enzymes. Ubiquitylating enzymes catalyze the conjugation of Ub molecules to host proteins to interfere with cellular signaling. Bacteria use the host E1 and E2 enzymes and their own E3 Ub ligases [11]. For example, SopA from *Salmonella typhimurium* mimics E6-AP Carboxyl Terminus (HECT)-type E3 ligases [16], and LubX from *Legionella pneumophila* mimics really interesting new gene (RING)-type E3 ligases [17]. Bacterial deubiquitylases (DUBs) remove Ub molecules (or Ub-linkages) against bacterial destruction. *Salmonella*, *Escherichia*, and *Shigella* possess DUB activity to cleave Ub-linkages [18] marked for foreign invaders by the host ubiquitylating machinery.

A recent study showed that SdeA, an enzyme belonging to the SidE effector family of *L. pneumophila*, transfers Ub to Rab-family proteins in an E1- and E2-independent manner [19]. Furthermore, the N-terminal region of SdeA has canonical DUB activity, indicating that this protein has a dual function as a ubiquitylation/deubiquitylation enzyme [20]. This novel E3 Ub ligase does not require ATP, which is a prerequisite for

conventional ubiquitylation [19]. The ATP-independent reaction is powered by nicotinamide adenine dinucleotide (NAD⁺) as a cofactor for ADP-ribosylation of Ub via Arg42 using the mono-ADP-ribosyltransferase (mART) domain of SdeA. The phosphodiesterase (PDE) domain then cleaves the phosphodiester bond of ADP and attaches phosphorylated Ub to the serine residue of protein substrates, which are usually Rab-family proteins associated with the endoplasmic reticulum [21].

ADP-ribosyltransferase (ART), an enzyme superfamily that catalyzes the NAD⁺-dependent ADP-ribosylation of proteins [22], is involved in many cellular processes including cell signaling, DNA repair, and gene regulation by using NAD⁺, a versatile metabolite that is at the center of a large array of biochemical processes [22]. The ART family is divided into three major clades according to consensus conserved residues: H-H-h, H-Y-[EDQ], and R-[ST]-EXE. The first histidine (H) and arginine (R) residues are involved in NAD⁺ binding; the aromatic residue (Y) and polar residues (S or T) are also involved in NAD⁺ binding; and the glutamate residue (E) is important for catalytic activity [23]. The EXE motif in the core of the ADP-ribosylation turn-turn (ARTT) loop in arginine-modifying enzymes is essential for catalysis as well as for protein substrate recognition [24]. Although the first Glu (Glu378 of iota-toxin) is required only for ART activity and not for NAD⁺ hydrolysis, the second Glu (Glu380 of iota-toxin) is essential for both ART and NAD⁺ hydrolysis activity [25]. Despite the contribution made by many structural studies of ART-family proteins to the classification of these enzymes into clades and identification of new members, the unique functions of each member of this diverse family remain to be determined.

The mART domain of SdeA from *Legionella* possesses conserved R-[ST]-EXE triad regions that are frequently found in bacterial ADP-ribosylating toxins. However, it remains unclear how the mART domain of SdeA catalyzes the NAD⁺-dependent attachment of the ADP-ribosyl moiety to the primary substrate, Ub. SdeA is a unique enzyme that possesses the mART domain, and the product of mART activity is targeted to the PDE domain within the molecule for the unusual ubiquitylation of the serine residue of substrates [21]. Therefore, biochemical and structural studies of the mART domain may contribute to our understanding of the mechanism underlying SdeA function, which will provide insight into novel Ub modifications and mART biology.

Results

Characterization of the mART domain

SdeA, a *L. pneumophila* effector protein, has four domains: an N-terminal DUB domain (residues 1–193),

a PDE domain, a mART domain, and a C-terminal putative coiled-coil (CC) domain (Fig. 1a). The molecular weight of full-length (FL) SdeA is approximately 180 kDa, and it is a monomer, as confirmed by size-exclusion chromatography coupled with multi-angle light scattering (SEC-MALS) (Fig. 1b). Among these domains, the mART domain plays an important role in the activity of SidE-family effectors during bacterial infection [19] and in the first ubiquitylation step leading to the formation of ADP-ribosylated Ub [21] (Fig. 1c). Therefore, we focused on investigating the mART domain of SdeA. However, the characterization of the domain was difficult based on amino acid sequences alone. To further understand the mART domain, several putative mART constructs were expressed and purified (Fig. 1d) based on the secondary structure prediction (Fig. S1). The reaction catalyzed by the mART domain of SdeA is the covalent attachment of ADP-ribose to the side-chain guanidine moiety of Arg42 of Ub [21] (Fig. 1c). The modification of Ub in each construct was examined using a Ub antibody that selectively recognizes the unmodified molecule [21]. Ub without any treatment was used as a negative control, and an SdeA H277A mutant lacking PDE activity (residues 226–905 covering both the PDE and mART domains) was used as a positive control for ADP-ribosylation of Ub [21]. To further dissect the mART domain, four different constructs were generated: L-mART (long-form, residues 531–905), mART (residues 595–905), S-mART (short-form, residues 655–905), and mART-C (residues 756–905). The mART-C contains the conserved R-S-EXE motif in the ARTT loop and is referred to as the mART domain in UniProt (<http://www.uniprot.org/uniprot/Q5ZTK4>). Treatment of these constructs with Ub and NAD⁺ showed that L-mART and mART domain constructs performed their functions adequately, whereas S-mART and mART-C constructs had no ADP-ribosylation activity (Fig. 1d). Detection of the ADP-ribosylated Ub fragment, a product of mART activity, by electrospray ionization (ESI) mass spectrometry confirmed the results (Fig. 1e). Therefore, the minimal region for ADP-ribosylation activity is located between residues 595 and 905, hereafter referred to as the mART domain.

Structure of the mART-C domain of SdeA

Only mART-C domain crystals were obtained despite attempts to crystallize all SdeA constructs (Fig. 1a). The putative NAD⁺-binding cleft is included in the mART-C domain [26]. Three crystal structures were resolved: the mART-C wild type (WT) and the catalytically inactive mutant (E860A/E862A) in the apo state, and the double mutant in complex with NAD⁺ (Table 1). The mART-C domain consists of three α -helices and seven β -strands in a mixture of α/β -folds with a β -sandwich and connecting loops

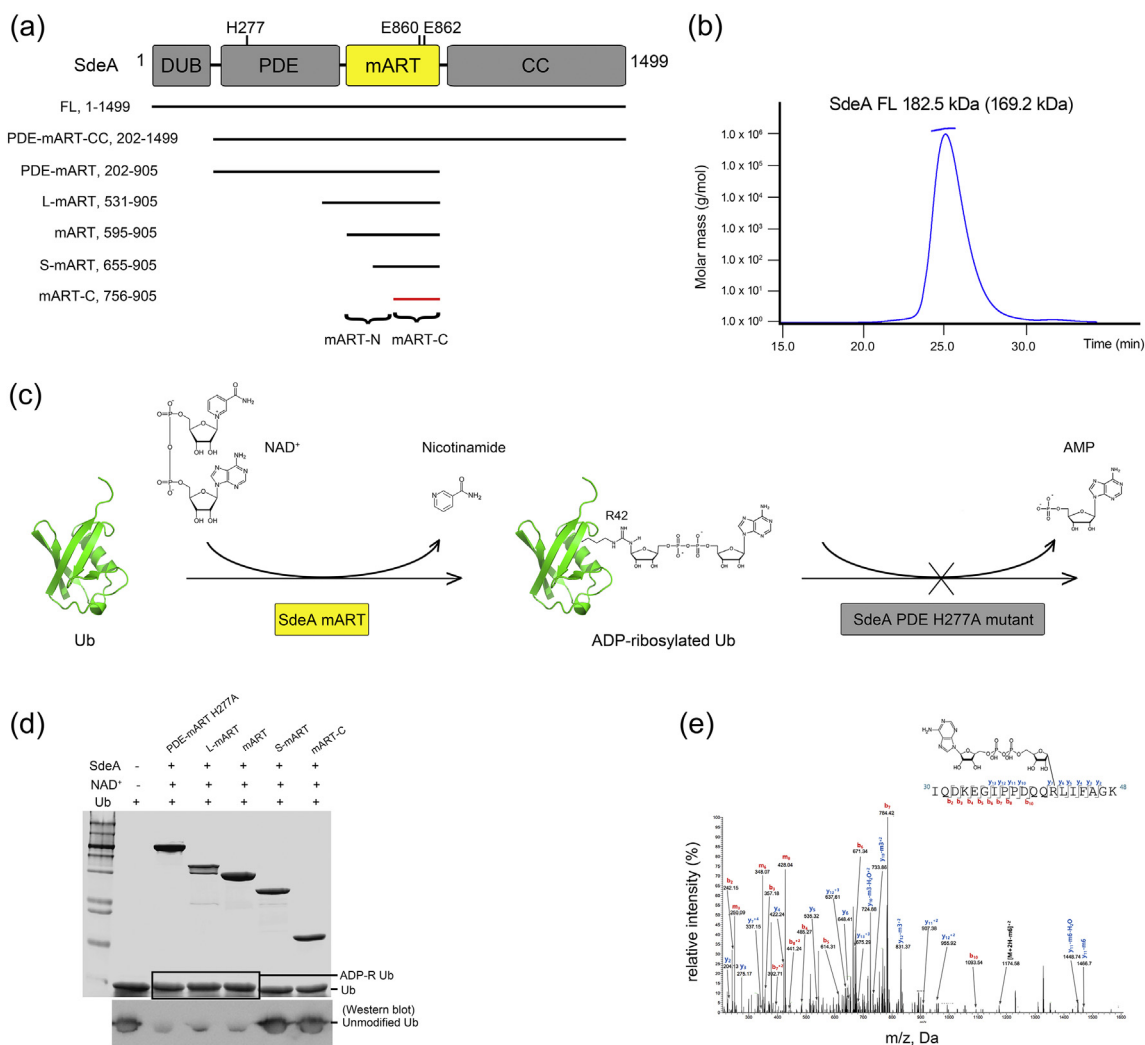


Fig. 1. Domain architecture of SdeA and ADP-ribosylation of Ub by mART. (a) Schematic representation of the domain organization of SdeA and the constructs (FL: 1–1499; PDE-mART-CC: 202–1499; PDE-mART: 202–905; L-mART (long-form): 531–905; mART: 595–905; S-mART (short-form): 655–905; mART-C: 756–905) used in the study. (b) The oligomeric state of FL SdeA was analyzed by SEC-MALS. The horizontal line represents the measured molecular mass (182.5 kDa) with the theoretically calculated molecular mass (169.2 kDa) value in parentheses. (c) Enzymatic reaction scheme of the mART domain of SdeA. The cofactor NAD⁺ is hydrolyzed into NCA and ADP-ribose, and the latter is covalently attached to the side chain nitrogen atom of Arg42 of Ub. The H277A mutant lacks PDE activity and the intermediate product, ADP-ribosylated Ub is obtained. (d) ADP-ribosylation of Ub was tested with several different constructs of SdeA. The PDE-mART H277A mutant was used as the positive control for ADP-ribosylation. The sizes of ADP-ribosylated Ub and unmodified Ub were slightly different in the 20% SDS-PAGE gel. The result was confirmed using a Ub antibody from Abcam that recognizes only unmodified Ub. (e) The site of Ub modification was determined by ESI mass spectrometry. HCD fragmentation spectrum of the ADP-ribosylated Ub tryptic peptide IQDKEGIPPDDQQLIFAGK. The $[M + 4H]^{4+}$ peak at $m/z = 674.57$ in the precursor mass scan was selected as a precursor ion for HCD fragmentation. ADP-ribosylated-specific product ions were detected at m/z 250.09 (adenosine-H₂O⁺), 348.07 [adenosine-mono phosphate⁺ (AMP⁺)], and 428.04 [adenosine-di phosphate⁺ (ADP⁺)].

(Fig. 2a). The β -sandwich core is packed in a four-stranded mixed β -sheet ($\beta 1$, $\beta 3$, $\beta 6$, and $\beta 7$) against a three-stranded antiparallel β -sheet ($\beta 4$, $\beta 5$, and $\beta 2$). The ARTT loop lies between $\beta 4$ and $\beta 5$, which is known to possess catalytic activity [24]. An apparent electron density was observed in the initial $F_o - F_c$ map of the NAD⁺-bound state between two β -sheets

(Fig. S2a). A ring structure of the nicotinamide (NCA) moiety of NAD⁺ was identified in the electron density, whereas no electron density was apparent for the rest of the NAD⁺ molecule (Fig. S2b). The binding pocket for NCA was clearly observed on the molecular surface (Fig. 2b). Although no electron density of the remaining ADP-ribose part was observed, the

Table 1. X-ray data collection and refinement statistics

| | EE/AA NCA complex | EE/AA apo | WT apo |
|---|------------------------------------|-----------------------|-----------------------|
| Data collection | | | |
| Beamlines | PF, BL-17A | SPring-8, BL44XU | SPring-8, BL44XU |
| Space group | C222 ₁ | P12 ₁ 1 | P12 ₁ 1 |
| Cell dimensions | | | |
| <i>a</i> , <i>b</i> , <i>c</i> (Å) | 37.9, 75.7, 84.7 | 43.8, 85.4, 70.8 | 44.0, 86.7, 71.0 |
| α , β , γ (°) | 90.0, 90.0, 90.0 | 90.0, 97.1, 90.0 | 90.0, 97.9, 90.0 |
| Wavelength (Å) | 0.97877 | 0.90000 | 0.90000 |
| Resolution (Å) | 50.0–1.55 (1.55–1.58) ^a | 50.0–2.40 (2.44–2.40) | 50.0–2.07 (2.11–2.07) |
| <i>R</i> _{merge} | 0.110 (0.542) | 0.119 (0.405) | 0.149 (0.881) |
| <i>I</i> / σ <i>I</i> | 32.4 (2.88) | 34.7 (16.01) | 16.5 (2.73) |
| Completeness (%) | 99.8 (100.0) | 99.2 (99.2) | 99.8 (98.5) |
| Redundancy | 6.7 (5.8) | 3.6 (3.6) | 4.0 (3.4) |
| SAD-phasing | | | |
| No. of Se atoms | 3 | | |
| FOM before/after DM | 0.27/0.35 | | |
| Refinement | | | |
| Resolution (Å) | 34.6–1.55 (1.60–1.55) | 32.4–2.40 (2.49–2.40) | 43.5–2.06 (2.13–2.06) |
| No. reflections | 18,142 (1,754) | 19,830 (1,741) | 32,455 (3,010) |
| <i>R</i> _{work} / <i>R</i> _{free} (%) | 20.4/24.6 | 18.5/26.1 | 22.5/27.0 |
| No. of atoms | 1182 | 4427 | 4476 |
| Protein | 1141 | 4308 | 4417 |
| Ligand | 9 | | |
| Water | 32 | 119 | 59 |
| <i>B</i> -factors (Å ²) | 27.08 | 28.17 | 33.27 |
| Protein | 27.03 | 28.12 | 33.34 |
| Ligand | 32.49 | | |
| Water | 27.25 | 30.05 | 28.30 |
| R.m.s. deviations | | | |
| Bond lengths (Å) | 0.016 | 0.013 | 0.003 |
| Bond angles (°) | 1.26 | 1.22 | 0.73 |
| Ramachandran (%) | | | |
| Favored | 96.53 | 95.90 | 96.34 |
| Allowed | 3.47 | 4.10 | 3.66 |
| Outliers | 0.00 | 0.00 | 0.00 |
| PDB ID | 5YSI | 5YSK | 5YSJ |

^a Values in parenthesis are the highest-resolution shell.

surrounding region of the NCA-binding pocket was covered by the positively charged surface, which might be important for NAD⁺ recognition.

The ARTT loop consisting of residues 852–862 was located near the NCA-bound region. Structural comparison between the NAD⁺-bound and apo states identified almost identical structures except for the ARTT loop (Fig. 2c). The loop in the NAD⁺-bound structure (E860A/E862A mutation within the ARTT motif) moves toward NAD⁺, which is in the closed state in which the glutamic acid residues catalyze the cleavage of NAD⁺ into NCA and ADP-ribose (Fig. 2d). However, the loop in the WT and EE/AA mutant in the apo state moves away from NAD⁺, adopting the open state in which the key residues are relatively far away from the NAD⁺ cleavage site. Therefore, ARTT loop flexibility plays a critical role in the cleavage of the NAD⁺ molecule.

The NAD⁺-binding site

Key residues important for mART function are well conserved, especially near NCA. The mART domain

of SdeA from *Legionella* belongs to the R-[ST]-EXE clade, and the corresponding residues are Arg766, Ser820, Thr821, Glu860, and Glu862 (Fig. 2d). Arg766 is located in the first β -strand and is involved in NAD⁺ binding. Although the exact mechanism could not be defined because of the absence of the ADP-ribose moiety, the positively charged Arg766 guanidine group likely interacts with the phosphate moiety of ADP based on the previously reported structures of iota-toxin and C3 exoenzyme [27, 28]. The side-chain carbon atoms of neighboring Ser820 and Thr821 located in the second β -strand make contact with the NCA moiety through hydrophobic interactions (Figs. 2d and S2c). In many ARTs, there is a serine residue immediately after -[ST]-, and the corresponding residue in SdeA was identified as a similar threonine residue, Thr822. A non-conserved residue, Trp832, is also involved in NCA ring binding (Fig. 2e) and acts in a manner similar to the phenylalanine residue frequently found at this position in the same clade. It has been reported [25] that the first glutamic acid residue in iota-toxin (corresponding Glu860 in SdeA) is required only for

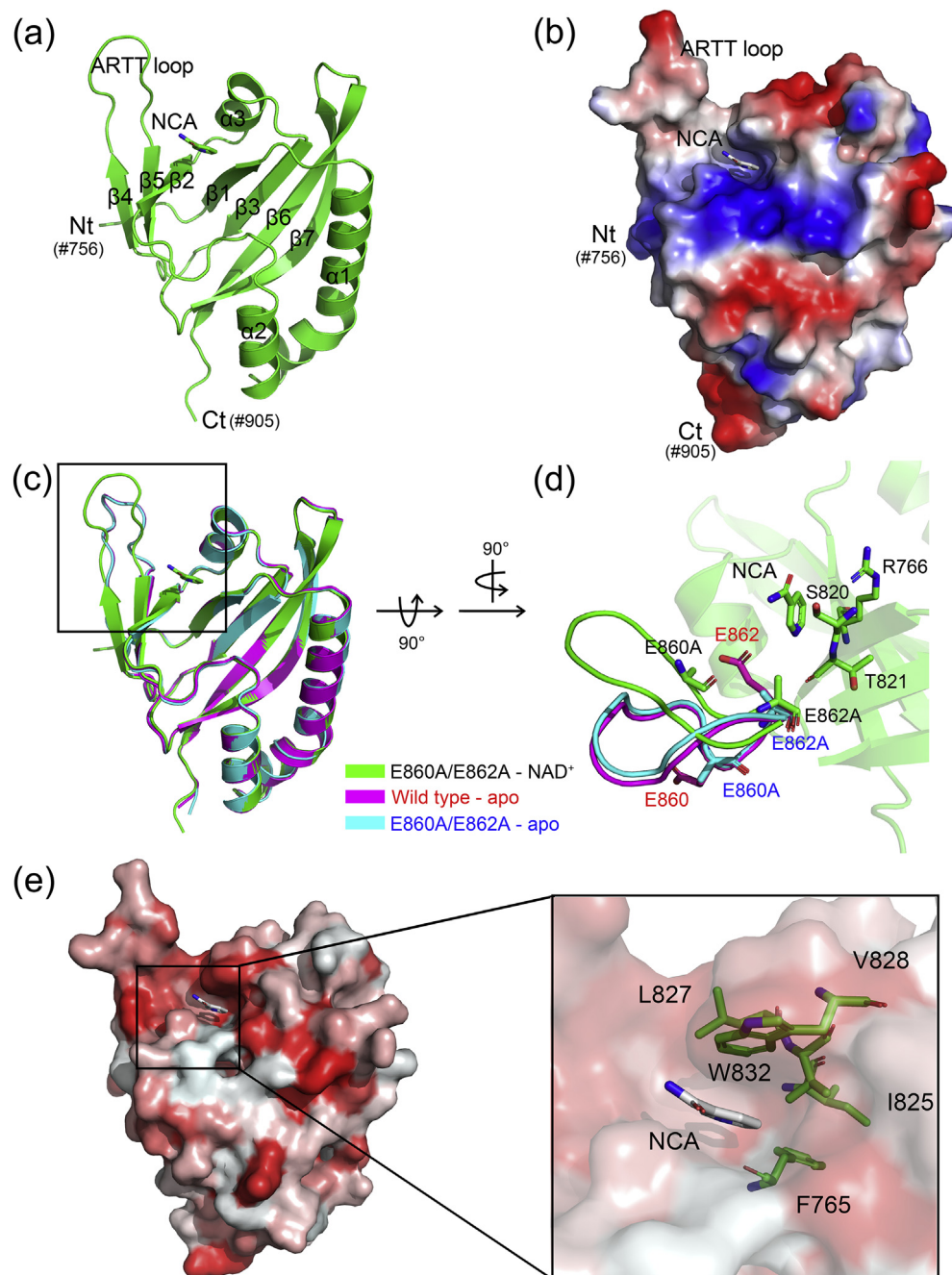


Fig. 2. Structure of the mART-C domain of SdeA. (a) Ribbon diagram of the mART-C domain with the bound NCA shown in stick model. Secondary structures are labeled in numerical order, and the important ARTT loop is indicated. N- and C-termini are also indicated as Nt and Ct, respectively, with the residue number in parenthesis. (b) A molecular surface with electrostatic potentials is shown. Positively and negatively charged surfaces are colored blue and red, respectively. NCA shown in stick model binds to the hydrophobic pocket. (c) Superimposition of mART-C domain structures in apo form and complexed with NAD⁺. The green ribbon represents E860A/E862A mutants complexed with NAD⁺, and magenta and cyan represent apo structures of the WT and E860A/E862A mutant, respectively. (d) Close-up view of the ARTT loop. Compared with the apo conformation, the ARTT loop of the NAD⁺-bound structure is located closer to the NAD⁺ site. (e) Molecular surface of mART representing the hydrophobic property. The strong red color indicates stronger hydrophobicity. The NCA-binding site is closed up, and the residues involved in hydrophobic contacts with NCA are labeled.

ART activity, whereas the second glutamic acid residue (Glu862 in SdeA) is essential for both ART and NAD⁺ hydrolysis activity.

The NCA ring binds to a hydrophobic pocket composed of Phe765, Ile825, Leu827, Val828, and Trp832 (Fig. 2e). A hydrophilic patch was observed on the surface of the mART-C domain connected to the hydrophobic pocket (Fig. 2b). This observation is consistent with data indicating that NCA requires a hydrophobic pocket for binding (Fig. S2c), whereas the remaining NAD⁺ sections require a hydrophilic patch. After NAD⁺ cleavage catalyzed by the mART domain, this pocket may not accommodate the NCA moiety, and ADP-ribose is transferred to the Ub molecule to avoid recombination [29, 30].

Comparison of the mART domain of SdeA with other ARTs

Compared with other ARTs, the mART-C domain of SdeA shares a similar folding pattern with conserved

β -strands [23], but differs in its structural details (Fig. 3). Structurally similar molecules were identified using the DALI server [31], including ART type III effector HopU1 from *Pseudomonas syringae* (PDB ID: 3U0J, Z = 9.5) [32], type III effector XopAl from *Xanthomonas axonopodis* (PDB ID: 4ELN, Z = 6.9), and the actin-targeting ART VahC from *Aeromonas hydrophila* (PDB ID: 4FML, Z = 6.7) [33]. Despite the similar structures, mART of SdeA is non-homologous in sequence to HopU1, XopAl, and VahC (11.5%, 9.3%, and 11.9% sequence identity, respectively). The N-terminal α -helical regions, particularly those from type III effectors, formed a compact structure with the NAD⁺-binding α/β -domain (Fig. 3b, c). The α -helical region of VahC appeared to be somewhat isolated from the NAD⁺-binding domain, despite several contacts between them (Fig. 3d). However, SdeA may contain a separate domain in its N-terminal region, which is predicted to adopt an α -helical structure (Fig. S1). These results combined with biochemical data (see following sections)

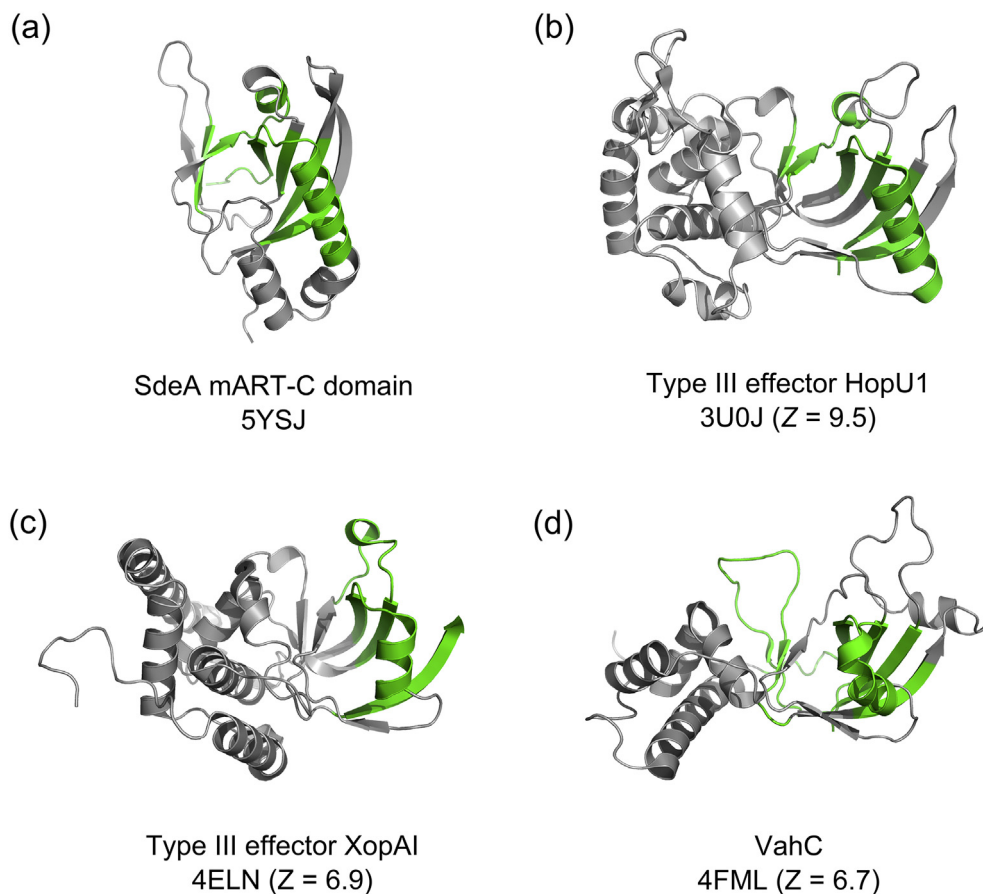


Fig. 3. Comparison of the overall structure of the mART-C domain of SdeA with those of other ARTs. Ribbon diagrams comparing the overall structures of SdeA (a), type III effector HopU1 (b), type III effector XopAl (c), and VahC, actin-targeting ART from *A. hydrophila* (d). This orientation was obtained by an approximately 30° clockwise rotation along the vertical axis from the view of Fig. 2a. Structural regions that match the corresponding region of SdeA are colored green in each structure. PDB ID codes and Z-scores from the DALI server for each structure are shown below each structure. There is significant contact between the N-terminal α -helical region (gray color) and the region structurally similar to mART-C (green color).

suggested that the mART domain of SdeA exists as two separate domains, herein termed mART-N (residues 595–755) and mART-C (residues 756–905). This structural comparison indicates that mART-N partly contributes to the enzymatic function of mART.

NADase and ADP-ribosylation activities of the mART domain of SdeA

The mART domain has dual NAD⁺ hydrolysis and ADP-ribosylation activity. Both reactions can be easily monitored by FPLC at an absorption wavelength of 260 nm. Incubation of Ub with SdeA mART (595–905) WT and NAD⁺ yielded NCA as a product of the NADase reaction (Figs. 1c and 4a). ADP-ribosylated Ub was detected at 260 nm (Fig. 4a), which was a higher absorption peak than that of unmodified Ub at the same concentration (Fig. 4). NADase activity was greatly reduced in the absence of the substrate Ub (Fig. 4b), suggesting that NAD⁺ hydrolysis and ADP-ribosylation are coupled reactions as observed for other ARTs [27, 34]. The EXE (Glu860 and Glu862) motif contains key residues for enzymatic activity, and the NADase and ADP-ribosylation reactions did not occur when glutamic acid residues were mutated to alanine (Fig. 4c). Glu862 is particularly important for NADase activity, and

therefore, mutation of this residue blocks both reactions. Glu860 is involved in ADP-ribosylation, and mutation of this residue may block ADP-ribosylation activity even in the presence of NADase activity. As shown in Fig. 3e, the hydrophobic Trp832 residue was important for accommodating the NCA molecule; however, the single mutation W832A did not have a marked effect on NADase activity (data not shown), which could be attributed to the marginal reduction of hydrophobic interactions (Fig. S2c). Mutation of additional residues (R766A/S820A/W832A) involved in the recognition of NAD⁺ abolished the production of NCA (Fig. 4d) similar to the effect of glutamic acid mutations (Fig. 4c). Regarding the mART-C domain (756–905) WT, both NADase and ADP-ribosylation activity were eliminated (Fig. 4e, f). The mART-C domain contains the catalytic glutamic acid residues Glu860 and Glu862 involved in the NADase reaction; however, the target molecule Ub is indispensable for the ADP-ribosylation reaction. Therefore, we next investigated the role of the mART-N domain of SdeA in Ub binding.

Binding of NAD⁺ and Ub to SdeA

To dissect the binding and catalytic activity of the mART domain for NAD⁺ and Ub, the binding

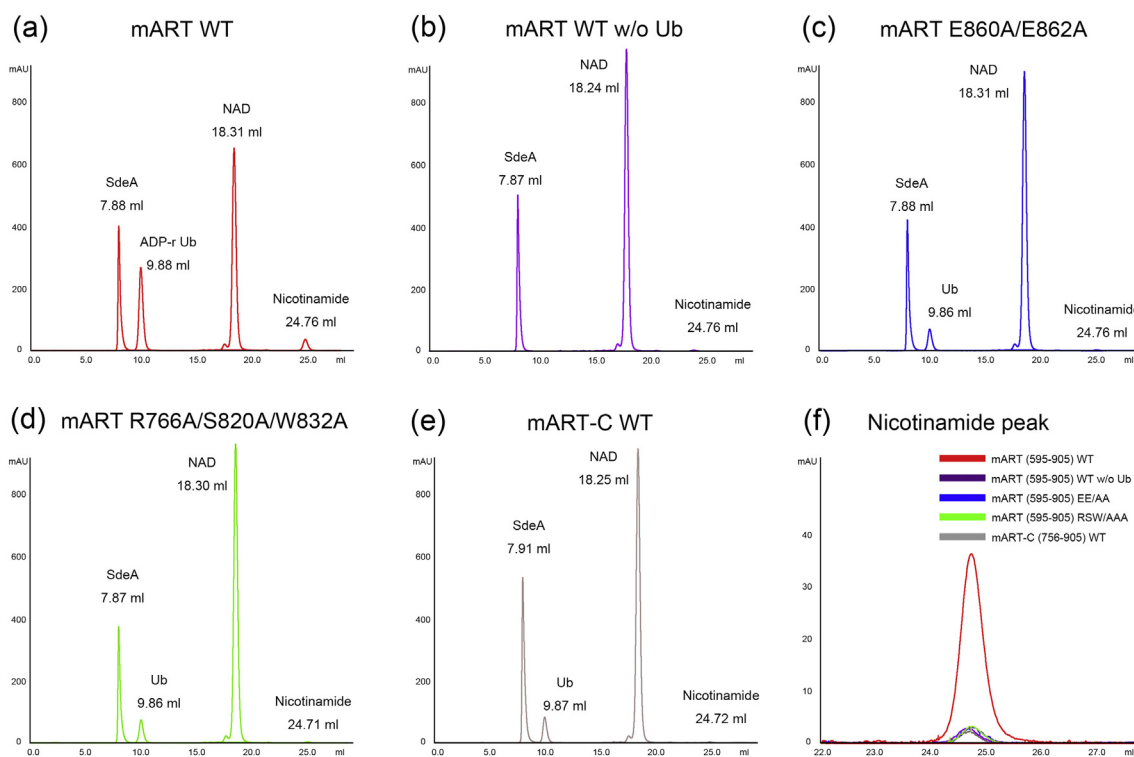


Fig. 4. *In vitro* ADP-ribosylation and NADase activity assay of the mART domain. FPLC analysis of the enzymatic products of mART WT (a), mART WT without Ub (b), mART E860A/E862E mutant (c), mART R766A/S820A/W832A mutant (d), and mART-C domain of SdeA (e). The elution positions of SdeA, ADP-ribosylated Ub (ADP-r Ub), Ub, NAD⁺, and NCA were confirmed by the standard. Note that the peak of ADP-r Ub in panel a is higher than that of unmodified Ub in panels c, d, and e. (f) The peaks for the NCA products for all panels (a–e) are amplified for clarity.

constants were measured using the surface plasmon resonance (SPR) technique. The mART domain (residues 595–905) and the mART-C domain (residues 756–905) were used as SdeA constructs. Both constructs showed similar binding constants for NAD^+ (Fig. 5a, b), which was consistent with the structural results showing that the mART-C domain of SdeA is mainly responsible for NAD^+ binding and hydrolysis. Structural analysis demonstrated that the catalytically important conserved residues Arg766, Ser820, Trp832, Glu860, and Glu862 of the mART-C domain are involved in interaction with and hydrolysis of NAD^+ (Fig. 2). This indicated that the mART-C domain is the minimal domain required for NADase activity, although the presence of the target substrate Ub is important for receiving the product of enzymatic activity, ADP-ribose (Fig. 4).

The binding constant was also measured using Ub as the substrate. Although the binding affinity for Ub was weak at a level of several hundred micromolar, it was within the range of affinity for Ub and Ub-binding proteins [35]. In contrast to NAD^+ , the mART and mART-C domains showed different binding constants for Ub. The K_D value of mART for Ub was approximately three times lower than that of mART-C (Fig. 4c, d), suggesting that the mART-N domain partly contributes to the recognition of Ub. The NADase and ADP-ribosylase results indicate that mART-C functions in NAD^+ binding and hydrolysis, and mART-N increases

the affinity of mART-C for Ub. Therefore, both domains utilize both NAD^+ and Ub molecule for efficient transfer of the ADP-ribose moiety.

Overall shape and spatial orientation of domains of SdeA

To investigate the exact molecular mechanism of SdeA, the structure of the FL SdeA protein needs to be resolved. To examine the structure of SdeA, purified samples of different length constructs were prepared (Fig. 1a). In parallel with extensive crystallization trials of these constructs, we performed small-angle X-ray scattering (SAXS) experiments (Table S1). SdeA showed a somewhat compact structure despite the multi-modular domains DUB-PDE-mART-CC of the enzyme (Fig. 6a). To further investigate the structure of SdeA, smaller constructs were examined by SAXS (Fig. S3a–j). Analysis of different combinations of molecular envelopes identified the locations of the DUB, PDE, mART, and CC regions in the FL structure (Fig. 6a–e). We found that the functionally isolated DUB domain at the N-terminal region does not exist as an isolated domain in the FL envelope (Fig. 6a). The PDE domain protrudes from the remaining mART-CC region (Fig. 6b). To confirm the location of the PDE domain, a SAXS experiment was performed using MBP-PDB-mART (MBP-tag at the N-terminus) (Fig. S4). An extra envelope was detected at the tip of the

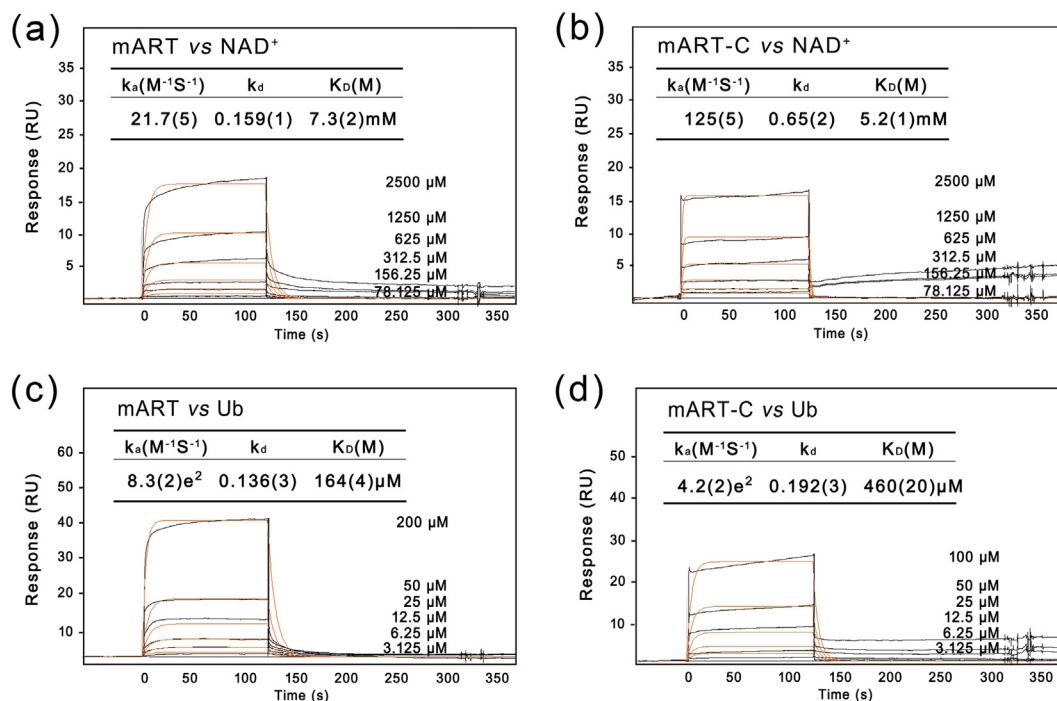


Fig. 5. Binding constant measurements by SPR. SPR sensorgrams for the binding of NAD^+ to immobilized mART (a) and mART-C (b) on the CM5 chip, and those for the binding of Ub to immobilized mART (c) and mART-C (d) on the same chip. Response (RU, resonance units) is plotted against time. The dissociation constant (K_D) was obtained by dividing the dissociation rate constant (k_d) by the association rate constant (k_a).

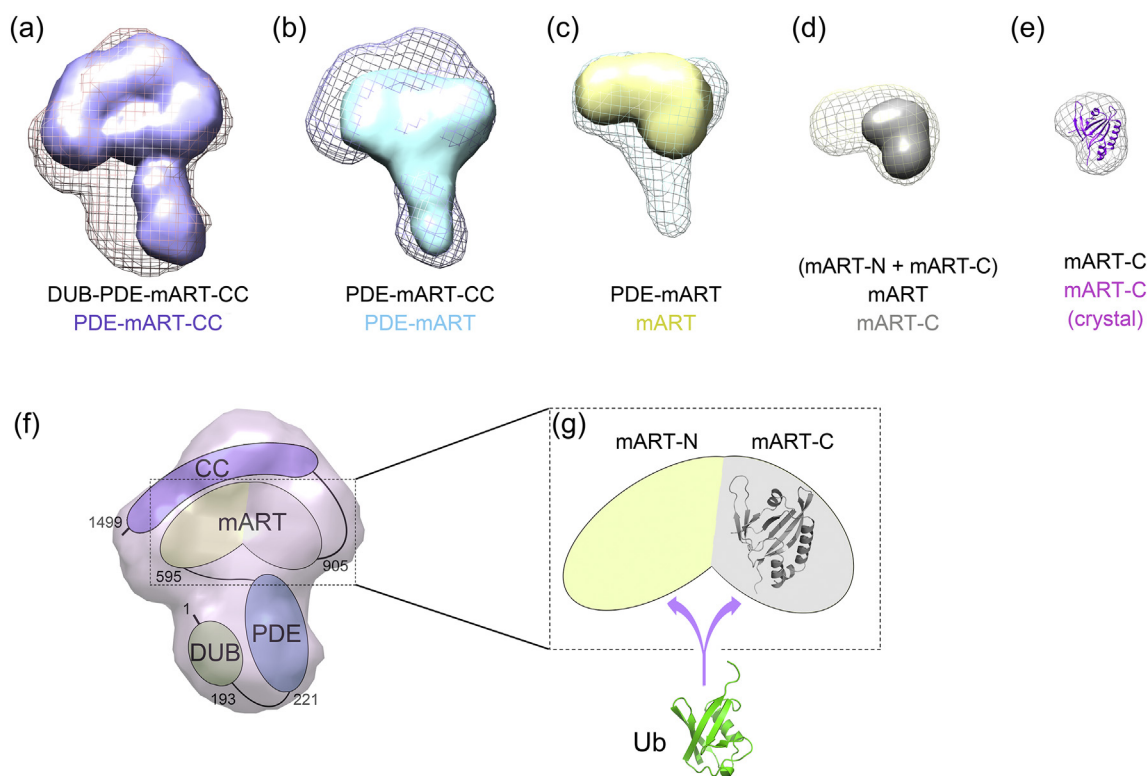


Fig. 6. Overall shape and spatial orientation of SdeA domains. (a) Molecular envelope of the FL SdeA (DUB-PDE-mART-CC) generated from SAXS data, which is represented as a mesh. The location of the DUB was identified by fitting the slate opaque molecular envelope of the PDE-mART-CC construct into the mesh molecular envelope of FL SdeA. (b) The molecular envelope of PDE-mART-CC is represented as a mesh to identify the CC domain in the C-terminus. The cyan opaque molecular envelope of the PDE-mART was fitted into the mesh molecular envelope of the PDE-mART-CC construct. (c) The yellow opaque molecular envelope of mART was fitted into the mesh molecular envelope of the PDE-mART construct. (d) The gray opaque molecular envelope of mART-C was fitted into the mesh molecular envelope of the mART construct. (e) The high-resolution crystal structure of mART-C (pink ribbon) was fitted into the low-resolution molecular envelope generated from SAXS data. (f) Spatial orientation of multi-modular domains in the overall shape of SdeA FL, which is shown as a transparent molecular envelope according to SAXS data. (g) Enlarged schematic model of the heart-shaped mART domain. In contrast to other ART structures, SdeA is characterized by separated mART-N and mART-C domains. The Ub molecule (green ribbon) interacts with both domains of mART, whereas NAD^+ interacts primarily with mART-C.

putative PDE domain, which shows a clear orientation of the domains in the molecular envelope. To better visualize the mART domain within FL SdeA, SAXS experiments using entire mART and the mART-C domain were performed. The mART consists of two separate domains with a heart shape (Fig. 6d).

Discussion

Ubiquitylation is an important protein modification involved in life and death processes in living organisms, and plays a role in the cellular defense against invading bacteria. *L. pneumophila* relies on the enigmatic molecule SdeA to remove Ub chains for its survival, as well as for ubiquitylating the host's Rab-family GTPases via a novel phosphoribose linkage on serine residues [19, 21]. Although the N-terminal DUB domain is well characterized [20], the detailed mechanisms underlying the function of the remaining multi-functional

domains PDE, mART, and CC remained elusive because of the lack of structural information.

The present SAXS data revealed the compact architecture of the ubiquitylating domains of SdeA (Fig. 6a–e). The SEC-MALS, SAXS envelope, and crystal structure data were used to propose a plausible model for FL SdeA (Fig. 6f). The C-terminal putative CC domain binds to the mART domain as a scaffold, which may affect the function of SdeA by regulating ADP-ribosylation activity. The mART domain is composed of two domains, mART-N and mART-C. The NAD^+ molecule is primarily recognized by mART-C and cleaved. Although mART-C has partial affinity for Ub, the α -helical mART-N domain also interacts with Ub to receive the cleaved ADP-ribose moiety at a specific position (Fig. 6g). The Arg42 on the surface of Ub is the target site, and both mART-N and mART-C may be important for the correct orientation of the Ub molecule. As shown in Fig. 4, the NADase and ADP-ribosylation activities are tightly coupled, suggesting that the

communication between mART-N and mART-C is critical for the function of SdeA. Furthermore, the binding affinity for Ub is weak, which is expected because ADP-ribosylated Ub needs to be cleaved by PDE and transferred to the substrate.

The location of the PDE domain near the mART domain is necessary for efficient enzymatic activity. SdeA attaches phosphoribosylated Ub to the serine residue(s) of Rab-family GTPases [21]; therefore, the substrate specificity for the ER-associated small GTPases Rab1, Rab6A, Rab30, and Rab33b may be determined by the PDE domain of SdeA, although this needs to be verified experimentally. This second reaction may be similar to the first mART reaction: the phosphodiester bond cleavage of ADP-ribosylated Ub and the covalent attachment to the target substrate Rab-family GTPase must be coupled. Therefore, similar to mART, enzymatically defective mutants such as H277A fail to produce phosphoribosylated Ub and AMP, resulting in the lack of transfer of phosphoribosylated Ub to the Rab-family GTPase. Similar to the affinity of the mART domain for Ub, that of SdeA for Rab-family GTPase must be very weak. It remains unclear whether the PDE domain is only involved in recognition of the GTPase substrates or if the mART domain is also involved in the recognition process with the PDE domain as in the case of mART-N and mART-C with regard to Ub. The next question is why only a subset of Rab-family GTPases can be recognized by SdeA, but not Rab5 and Rac1 [19]. To answer this question, we need structural information on the complex between SdeA and the target GTPase. Notwithstanding, the present results on the collaboration between mART-N and mART-C domain for efficient enzymatic reaction, the high-resolution structure of mART-C domain in complex with NAD⁺ ligand, and spatial orientation of modular domains in overall shape of SdeA constitute an initial step toward improving our understanding of how *Legionella* interferes with host defense signaling by means of the novel Ub modification mediated by SdeA.

Experimental Procedures

Sample preparation

The *SdeA* gene was amplified from *L. pneumophila* genomic DNA using standard PCR methods. The amplified PCR products were treated with the restriction enzymes, BamHI and KpnI and inserted into modified pETDuet-1 vectors (Novagen, 71146-3) including tobacco etch virus and thrombin cleavage sites for N-terminal hexa-histidine- or MBP (maltose-binding protein)-tagged protein. The plasmids were transformed into *Escherichia coli* BL21(DE3) cells. The QuikChange site-directed mutagenesis method (Stratagene) was used to prepare constructs expressing the SdeA mutants (H277A, R766A, S820A,

W832A, E860A, E862A, and E860S). Protein expression of the His-tagged constructs (SdeA FL, PDE-mART-CC, PDE-mART, mART, and mART-C) was induced by addition of 0.5 mM IPTG at 18 °C for 18 h. Cells were harvested by centrifugation and resuspended in 50 mM Tris-HCl buffer (pH 8.0) containing 100 mM NaCl and 1 mM TCEP [tris(2-carboxyethyl) phosphine hydrochloride]. The resuspended cells were disrupted by sonication. The cell lysate was loaded onto a HisTrap™ column (GE Healthcare, 17-5255-01), and eluted using a linear gradient of imidazole concentrations (0–500 mM). The affinity tag was cleaved using the tobacco etch virus protease (lab made) by overnight incubation at 4 °C, and the target protein was further purified by ion-exchange column chromatography using a HiTrap™ Q FF column (GE Healthcare, 17-5156-01) and eluted using a linear gradient of NaCl concentrations (0–1.0 M). Finally, the protein was loaded onto a HiLoad™ 16/600 Superdex™ 75pg (GE Healthcare, 28-9893-33) or Superdex™ 200pg (GE Healthcare, 28-9893-35) gel filtration column pre-equilibrated with 10 mM Tris-HCl (pH 8.0) containing 100 mM NaCl and 1 mM TCEP. For purification of MBP-PDE-mART-CC, cell lysates were applied to a column containing amylose resin (NEB). The beads were washed with at least five column volumes of buffer containing 50 mM Tris-HCl (pH 8.0), 100 mM NaCl, and 1 mM TCEP, and the MBP-fusion protein was eluted with the same buffer supplemented with 10 mM maltose. The remaining steps were the same as those described for other His-tagged constructs.

Crystallization and data collection

The purified SdeA WT or mutant was concentrated to approximately 10–20 mg/ml and crystallized at 22 °C using the sitting drop vapor diffusion method. The best crystals of the SdeA mART-C domain were obtained by mixing 1 µl of protein with 1 µl of reservoir solution containing 37%–42% (v/v) PEG400 (Hampton Research, HR2-603) and 100 mM MES-NaOH (pH 6.0). For the NAD complex, SdeA was co-crystallized in the presence of 5–30 mM NAD⁺ trihydrate (GoldBio, N-030-10). Crystals were cryoprotected by adding 15% (w/v) glycerol and then frozen in liquid nitrogen.

X-ray data of SdeA mART-C WT and E860A/E862A double mutant in the apo state were collected at beamline BL44XU, SPring-8, Japan, and beamline 5C, Pohang Accelerator Laboratory, South Korea, respectively. Crystals of the NAD⁺-bound selenomethionine-derivatized SdeA mART-C, the double mutant, were diffracted to 1.55-Å resolution, and the data were collected at beamline BL-17A, Photon Factory, Japan. The data sets were integrated, and scaling was performed using HKL2000 software [36]. Statistics for the collected data are summarized in Table 1.

Structure determination and refinement

Crystals of SdeA mART-C WT in the apo state were initially obtained. Although both single-wavelength anomalous dispersion (SAD) and multi-wavelength anomalous dispersion data sets up to 2.1-Å resolution were collected, we could not solve the structure of SdeA mART-C WT. This could be attributed to the presence of translational non-crystallographic symmetry (tNCS) in this crystal form, which might be originated from the multiple conformations of the catalytic loop (or ARTT loop) containing catalytic glutamic acids in four molecules of mART-C in the asymmetric unit. To solve this problem, the double mutant E860A/E862A was generated to inhibit NAD⁺ hydrolysis in the complex crystals. This mutant was crystallized in the same space group, and the crystal also showed tNCS. The mutant in complex with NAD⁺ was crystallized in the different space group *C*222₁ and diffracted to a resolution of 1.55 Å. The resulting complex crystal had no tNCS problem, and the structure was solved by SAD using a selenomethionine-derivatized protein. The initial phases were obtained using a Se-SAD data set; the model was rebuilt manually using COOT [37], and refinement was performed using PHENIX [38]. The phases of tNCS-containing data sets were successfully determined by molecular replacement using the refined coordinates of the NAD⁺ complexed SdeA mART-C domain mutant. All final models of the SdeA mART-C domain were validated using MolProbity [39]. Statistics for the refinement are summarized in Table 1. Structure comparisons were performed using the DALI server (<http://ekhidna2.biocenter.helsinki.fi/dali/>), and all structural figures were drawn using PyMOL (<http://www.pymol.org/>).

SEC-MALS

SEC-MALS experiments were performed using a fast protein liquid chromatography system (GE Healthcare) connected to a Wyatt MiniDAWN TREOS MALS instrument and Wyatt Optilab rEX differential refractometer. The buffers used were the same as those used in the final purification step, and the purified protein was loaded onto a SuperdexTM 200 Increase 10/300 GL (28-9909-44) gel filtration column. Ovalbumin was used as the isotropic scatterer for detector normalization. Light scattering from SdeA FL (5 mg/ml, 0.5 ml) was measured and analyzed using ASTRA V software (Wyatt).

Mass spectrometry

Tryptic digest samples were analyzed with a Q Exactive Plus mass spectrometer (Thermo Fisher Scientific, Bremen, Germany). Nanoliter-flow RPLC separations were performed on the Ultimate 3000 RSLCnano system (Thermo Fisher Scientific, San Jose, CA, USA). The Q Exactive Plus mass

spectrometer was set to a data-dependent acquisition mode to automatically switch between full scan MS (resolution of 70,000) and 10 MS/MS (HCD; resolution of 35,000) acquisitions with a dynamic exclusion duration of 25 s. All mass spectrometric data were obtained with Xcalibur v.2.2 software (Thermo Fisher Scientific, San Jose, CA, USA). Peptide sequences were assigned using Proteome Discoverer (version 2.2; Thermo Fisher Scientific, San Jose, CA, USA) with the SEQUEST HT search engine and the human UniProt/Swiss-Prot database (release 2017_10; 26,237 entries). The following search parameters were used: precursor ion mass tolerance of 10 parts per million, fragment ion mass tolerance of 0.02 Da, false discovery rate of 1% and peptide-spectrum matching false discovery rate of 5%, and methionine oxidation and arginine ADP-ribosylation as variable modifications.

NADase and ADP-ribosylation activity assays

Samples were prepared by adding NAD⁺ to Ub and incubation at 37 °C for 2 h. The NADase activity assay was performed using the HPLC-equipped SuperdexTM 30 increase column (GE Healthcare, 29219757) and FPLC-equipped HypersilTM BDS C18 columns (Thermo Fisher, 28105-124630), with 20 mM Hepes (pH 7.5) buffer containing 150 mM NaCl and 1 mM TCEP at room temperature. The pure ligands, NAD⁺, and NCA alone were analyzed as controls.

SPR

The binding affinity of NAD⁺ or Ub to SdeA (mART or mART-C domain) WT and mutants was measured using a Biacore T200 apparatus and phosphate-buffered saline. Initially, SdeA proteins were immobilized on series S sensor chip CM5 surfaces using the standard amine coupling procedure. Various concentrations of NAD⁺ (78.125–2500 μM) or Ub (3.125–200 μM) were then injected at 30 μl/min over the chip. The response of NAD⁺ or Ub was calculated by subtracting that of the blank flow cell. All experiments were performed multiple times. Data were calculated using Scrubber2 software.

SAXS

For SAXS coupled with a size-exclusion column (SEC-SAXS), proteins (SdeA FL, PDE-mART-CC, MBP-PDE-mART-CC, PDE-mART, mART, and mART-C) were loaded onto a SuperdexTM 200 Increase 10/300 GL column (GE Healthcare, 28-9909-44) and eluted with buffer containing 50 mM MES (pH 6.0), 200 mM NaCl, 1 mM TCEP, and 5% (w/v) glycerol. Conventional SAXS experiments were performed for the PDE-mART protein prepared using the same gel filtration conditions, and the protein was diluted serially from 12.5 to 3.2 mg/ml. All scattering

data were measured at beamline BL-10C, Photon Factory, Japan [40]. PILATUS3 2M (DECTRIS, Switzerland) was used as the X-ray detector. Data were collected using radiation at a wavelength of 1.5 Å and a sample-detector distance of 3.0 m. Approximately 5–10 mg of SdeA proteins was loaded onto the gel filtration column for SEC-SAXS experiments. An X-ray scattering measurement at a frame rate of 20.001 s (exposure time: 20 s) was started when the protein concentration began to increase. Data from the detector were normalized, averaged, buffer subtracted, and placed on an absolute scale relative to water, according to standard procedures. Scattering data from STATIC were averaged circularly. Raw data from SEC-SAXS were processed by CHROMIXS (ATSAS program suite) and subjected to analysis with the software package PRIMUS (ATSAS program suite), which provided the radius of gyration (R_g), Porod volume, and experimental molecular weight [41]. An indirect Fourier transform of the scattering curve $I(s)$ calculated by GNOM was used to obtain the distance distribution function $P(r)$ and the maximum particle dimensions D_{max} [42]. *Ab initio* modeling and averaging of these models were performed using DAMMIF. A SAXS electron envelope map from the *ab initio* DAMMIF model was generated using Chimera [43]. Statistics for the SAXS experimental results are summarized in Table S1.

Accession numbers

The atomic coordinates and structural factors have been deposited in the Protein Data Bank under the PDB ID codes 5YSI (NCA complex), 5YSK (EE/AA apo), and 5YSJ (WT apo).

Acknowledgments

We thank the staff at beamline 5C, Pohang Accelerator Laboratory, Republic of Korea, and beamline BL-17A, Photon Factory, Japan, for their help with the X-ray data collection. This work was in part performed under the International Collaborative Research Program of Institute for Protein Research, Osaka University (ICR-17-05). Diffraction data were collected at the Osaka University beamline BL44XU at SPring-8 (Harima, Japan; Proposal Nos. 2017A6775 and 2017B6775). We also thank the staff at beamline BL-10C, Photon Factory, Japan, for their help with the SAXS data collection. L.K. is a recipient of a POSCO Science Fellowship of POSCO TJ Park Foundation. This research was supported by a grant from the Samsung Science & Technology Foundation (SSTF-BA 1701-14).

Author Contributions: L.K., D.H.K., B.H.K., and M.R.P. prepared samples; L.K. generated crystals

and solved structures; L.K. and D.H.K. performed SAXS experiments; L.K. and B.H.K. performed biochemical assays; L.K., D.H.K., and H.K.S. designed experiments; L.K. and H.K.S. analyzed the data and wrote the manuscript.

Conflict of Interest Statement: The authors declare that they have no conflicts of interest.

Note added in proof: Very recently, four independent research groups reported X-ray structures of larger construct of SidE-family protein than current study [44–47].

Appendix A. Supplementary data

Supplementary data to this article can be found online at <https://doi.org/10.1016/j.jmb.2018.05.043>.

Received 19 April 2018;

Received in revised form 24 May 2018;

Accepted 27 May 2018

Available online 2 June 2018

Keywords:

Legionella pneumophila;
mART;
NAD⁺;
SdeA;
ubiquitin

Abbreviations used:

ART, ADP-ribosyltransferase; ARTT, ADP-ribosylation turn–turn; DUB, deubiquitylase; CC, coiled-coil; ESI, electrospray ionization; FL, full-length; MBP, maltose-binding protein; mART, mono-ADP-ribosyltransferase; NAD⁺, nicotinamide adenine dinucleotide; NCA, nicotinamide; PDE, phosphodiesterase; SAD, single-wavelength anomalous diffraction; SAXS, small-angle X-ray scattering; SEC-MALS, size-exclusion chromatography with a multi-angle light scattering; SPR, surface plasmon resonance; TCEP, tris(2-carboxyethyl)phosphine hydrochloride; tNCS, translational non-crystallographic symmetry; Ub, ubiquitin; WT, wild-type.

References

- [1] D. Komander, M. Rape, The ubiquitin code, *Annu. Rev. Biochem.* 81 (2012) 203–229.
- [2] Y.T. Kwon, A. Ciechanover, The ubiquitin code in the ubiquitin–proteasome system and autophagy, *Trends Biochem. Sci.* 42 (2017) 873–886.
- [3] A. Varshavsky, The ubiquitin system, autophagy, and regulated protein degradation, *Annu. Rev. Biochem.* 86 (2017) 123–128.
- [4] A. Hershko, A. Ciechanover, The ubiquitin system, *Annu. Rev. Biochem.* 67 (1998) 425–479.
- [5] B.A. Schulman, Twists and turns in ubiquitin-like protein conjugation cascades, *Protein Sci.* 20 (2011) 1941–1954.
- [6] A. Varshavsky, The ubiquitin system, an immense realm, *Annu. Rev. Biochem.* 81 (2012) 167–176.

- [7] K.N. Swatek, D. Komander, Ubiquitin modifications, *Cell Res.* 26 (2016) 399–422.
- [8] D.H. Kwon, H.K. Song, A structural view of xenophagy, a battle between host and microbes, *Mol. Cell* 41 (2018) 27–34.
- [9] I. Dikic, Proteasomal and autophagic degradation systems, *Annu. Rev. Biochem.* 86 (2017) 193–224.
- [10] D.J. Klionsky, B.A. Schulman, Dynamic regulation of macroautophagy by distinctive ubiquitin-like proteins, *Nat. Struct. Mol. Biol.* 21 (2014) 336–345.
- [11] Y. Zhou, Y. Zhu, Diversity of bacterial manipulation of the host ubiquitin pathways, *Cell. Microbiol.* 17 (2015) 26–34.
- [12] P. Munro, G. Flatau, E. Lemichez, Bacteria and the ubiquitin pathway, *Curr. Opin. Microbiol.* 10 (2007) 39–46.
- [13] M. Llosa, C. Roy, C. Dehio, Bacterial type IV secretion systems in human disease, *Mol. Microbiol.* 73 (2009) 141–151.
- [14] J. Qiu, Z.Q. Luo, Hijacking of the host ubiquitin network by *Legionella pneumophila*, *Front. Cell. Infect. Microbiol.* 7 (2017) 487.
- [15] T. Maculins, E. Fiskin, S. Bhogaraju, I. Dikic, Bacteria–host relationship: ubiquitin ligases as weapons of invasion, *Cell Res.* 26 (2016) 499–510.
- [16] Y. Zhang, W.M. Higashide, B.A. McCormick, J. Chen, D. Zhou, The inflammation-associated *Salmonella* SopA is a HECT-like E3 ubiquitin ligase, *Mol. Microbiol.* 62 (2006) 786–793.
- [17] T. Kubori, A. Hyakutake, H. Nagai, *Legionella* translocates an E3 ubiquitin ligase that has multiple U-boxes with distinct functions, *Mol. Microbiol.* 67 (2008) 1307–1319.
- [18] J.N. Pruneda, C.H. Durkin, P.P. Geurink, H. Ovaa, B. Santhanam, D.W. Holden, et al., The molecular basis for ubiquitin and ubiquitin-like specificities in bacterial effector proteases, *Mol. Cell* 63 (2016) 261–276.
- [19] J. Qiu, M.J. Sheedlo, K. Yu, Y. Tan, E.S. Nakayasu, C. Das, et al., Ubiquitination independent of E1 and E2 enzymes by bacterial effectors, *Nature* 533 (2016) 120–124.
- [20] M.J. Sheedlo, J. Qiu, Y. Tan, L.N. Paul, Z.Q. Luo, C. Das, Structural basis of substrate recognition by a bacterial deubiquitinase important for dynamics of phagosome ubiquitination, *Proc. Natl. Acad. Sci. U. S. A.* 112 (2015) 15090–15095.
- [21] S. Bhogaraju, S. Kalayil, Y. Liu, F. Bonn, T. Colby, I. Matic, et al., Phosphorylation of ubiquitin promotes serine ubiquitination and impairs conventional ubiquitination, *Cell* 167 (2016) 1636–1649 (e13).
- [22] L. Aravind, D. Zhang, R.F. de Souza, S. Anand, L.M. Iyer, The natural history of ADP-ribosyltransferases and the ADP-ribosylation system, *Curr. Top. Microbiol. Immunol.* 384 (2015) 3–32.
- [23] M.O. Hottiger, P.O. Hassa, B. Luscher, H. Schuler, F. Koch-Nolte, Toward a unified nomenclature for mammalian ADP-ribosyltransferases, *Trends Biochem. Sci.* 35 (2010) 208–219.
- [24] S. Han, J.A. Tainer, The ARTT motif and a unified structural understanding of substrate recognition in ADP-ribosylating bacterial toxins and eukaryotic ADP-ribosyltransferases, *Int. J. Med. Microbiol.* 291 (2002) 523–529.
- [25] H. Barth, J.C. Preiss, F. Hofmann, K. Aktories, Characterization of the catalytic site of the ADP-ribosyltransferase *Clostridium botulinum* C2 toxin by site-directed mutagenesis, *J. Biol. Chem.* 273 (1998) 29506–29511.
- [26] S. Han, J.A. Craig, C.D. Putnam, N.B. Carozzi, J.A. Tainer, Evolution and mechanism from structures of an ADP-ribosylating toxin and NAD complex, *Nat. Struct. Biol.* 6 (1999) 932–936.
- [27] T. Tsurumura, Y. Tsumori, H. Qiu, M. Oda, J. Sakurai, M. Nagahama, et al., Arginine ADP-ribosylation mechanism based on structural snapshots of iota-toxin and actin complex, *Proc. Natl. Acad. Sci. U. S. A.* 110 (2013) 4267–4272.
- [28] J. Menetrey, G. Flatau, E.A. Stura, J.B. Charbonnier, F. Gas, J.M. Teulon, et al., NAD binding induces conformational changes in Rho ADP-ribosylating *Clostridium botulinum* C3 exoenzyme, *J. Biol. Chem.* 277 (2002) 30950–30957.
- [29] P.J. Berti, S.R. Blanke, V.L. Schramm, Transition state structure for the hydrolysis of NAD catalyzed by diphtheria toxin, *J. Am. Chem. Soc.* 119 (1997) 12079–12088.
- [30] S. Han, A.S. Arvai, S.B. Clancy, J.A. Tainer, Crystal structure and novel recognition motif of rho ADP-ribosylating C3 exoenzyme from *Clostridium botulinum*: structural insights for recognition specificity and catalysis, *J. Mol. Biol.* 305 (2001) 95–107.
- [31] L. Holm, L.M. Laakso, Dali server update, *Nucleic Acids Res.* 44 (2016) W351–W355.
- [32] B.R. Jeong, Y. Lin, A. Joe, M. Guo, C. Korneli, H. Yang, et al., Structure function analysis of an ADP-ribosyltransferase type III effector and its RNA-binding target in plant immunity, *J. Biol. Chem.* 286 (2011) 43272–43281.
- [33] A. Shniffer, D.D. Visschedyk, R. Ravulapalli, G. Suarez, Z.J. Turgeon, A.A. Petrie, et al., Characterization of an actin-targeting ADP-ribosyltransferase from *Aeromonas hydrophila*, *J. Biol. Chem.* 287 (2012) 37030–37041.
- [34] J. van Damme, M. Jung, F. Hofmann, I. Just, J. Vandekerckhove, K. Aktories, Analysis of the catalytic site of the actin ADP-ribosylating *Clostridium perfringens* iota toxin, *FEBS Lett.* 380 (1996) 291–295.
- [35] J.H. Hurley, S. Lee, G. Prag, Ubiquitin-binding domains, *Biochem. J.* 399 (2006) 361–372.
- [36] Z. Otwinowski, W. Minor, Processing of X-ray diffraction data collected in oscillation mode, *Methods Enzymol.* 276 (1997) 307–326.
- [37] P. Emsley, B. Lohkamp, W.G. Scott, K. Cowtan, Features and development of Coot, *Acta Crystallogr. D Biol. Crystallogr.* 66 (2010) 486–501.
- [38] P.D. Adams, P.V. Afonine, G. Bunkoczi, V.B. Chen, I.W. Davis, N. Echols, et al., PHENIX: a comprehensive Python-based system for macromolecular structure solution, *Acta Crystallogr. D Biol. Crystallogr.* 66 (2010) 213–221.
- [39] V.B. Chen, W.B. Arendall III, J.J. Headd, D.A. Keedy, R.M. Immormino, G.J. Kapral, et al., MolProbity: all-atom structure validation for macromolecular crystallography, *Acta Crystallogr. D Biol. Crystallogr.* 66 (2010) 12–21.
- [40] N. Igarashi, Y. Watanabe, Y. Shinohara, Y. Inoko, G. Matsuba, H. Okuda, et al., Upgrade of the small angle X-ray scattering beamlines at the Photon Factory, *J. Phys. Conf. Ser.* 272 (2011).
- [41] M.V. Petoukhov, D. Franke, A.V. Shkumatov, G. Tria, A.G. Kikhney, M. Gajda, et al., New developments in the ATSAS program package for small-angle scattering data analysis, *J. Appl. Crystallogr.* 45 (2012) 342–350.
- [42] A.V. Semenyuk, D.I. Svergun, GNOM—a program package for small-angle scattering data processing, *J. Appl. Crystallogr.* 24 (1991) 537–540.
- [43] E.F. Pettersen, T.D. Goddard, C.C. Huang, G.S. Couch, D.M. Greenblatt, E.C. Meng, et al., UCSF Chimera—a visualization system for exploratory research and analysis, *J. Comput. Chem.* 25 (2004) 1605–1612.
- [44] Y. Dong, Y. Mu, Y. Xie, Y. Zhang, Y. Han, Y. Zhou, et al., Structural basis of ubiquitin modification by the *Legionella* effector SdeA, *Nature* 557 (2018) 674–678.

-
- [45] S. Kalayil, S. Bhogaraju, F. Bonn, D. Shin, Y. Liu, N. Gan, et al., Insights into catalysis and function of phosphoribosyl-linked serine ubiquitination, *Nature* 557 (2018) 734–738.
- [46] A. Akturk, D.J. Wasilko, X. Wu, Y. Liu, Y. Zhang, J. Qiu, et al., Mechanism of phosphoribosyl-ubiquitination mediated by a single *Legionella* effector, *Nature* 557 (2018) 729–733.
- [47] Y. Wang, M. Shi, H. Feng, Y. Zhu, S. Liu, A. Gao, P. Gao, Structural insights into non-canonical ubiquitination catalyzed by SidE, *Cell* 173 (2018) 1231–1243.